Dalton Transactions

Accepted Manuscript

ROYAL SOCIETY OF CHEMISTRY

www.rsc.org/dalton

Journal Name

RSCPublishing

ARTICLE

The Origin of *Exo*-Selectivity in Methyl Cyanoformate Addition onto the C=C Bond of Norbornene in Pd-Catalyzed Cyanoesterification

Yasuhiro Okuda,[a] Robert K. Szilagyi,[b,c] Seiji Mori[*c] and Yasushi Nishihara[*a,d]

Cite this: DOI: 10.1039/x0xx00000x

Received 00th January 2012,
Accepted 00th January 2012

DOI: 10.1039/x0xx00000x

www.rsc.org/

A computational investigation has been carried out to elucidate the origin of the exclusive *exo*-selectivity in the Pd-catalyzed cyanoesterification of strained cyclic olefins, such as norbornene and norbornadiene. A hybrid density functional was selected for the level of theory with triple-ζ quality basis set, which was proposed in an earlier study to provide experimentally sound ground state electronic structure description for palladium(II) and palladium(IV) complexes from multi-edge X-ray absorption spectroscopic measurements. Given that the product of oxidative addition can be isolated, we focused on the olefin coordination as the earliest possible origin of *exo*-selectivity. The calculated geometric structure for the *trans*-Pd(CN)(COOR)$(PPh_3)_2$ complex at the BHandHLYP/def2TZVP/PCM(toluene) level is in an excellent agreement with its experimental structure from crystallographic measurements. Upon dissociation of one of its phosphane ligands, the coordinatively unsaturated *trans*-isomer is only 17 kJ mol^{-1} away from the isomerization transition state leading to the 14-electron *cis*-isomers that are 17 to 37 kJ mol^{-1} lower in energy than the *trans*-isomer. Regardless of the starting complex for olefin coordination, the *exo*-isomer for the norbornene complex is at least 23 kJ mol^{-1} lower than the corresponding *endo*-isomer. The origin of this considerable difference in Gibbs free energy can be attributed to the remarkably different steric and agostic hydrogen interactions between the methylene and the ethylene bridges of the norbornene and the adjacent *cis*-ligands at the Pd^{II} center.

Introduction

The Pd-catalyzed cyanoesterification of norbornene (NBE) and norbornadiene (NBD) have been developed[1] to provide a selective method for addition of cyano and ester groups onto C=C bonds through C–C bond cleavage.[2] This double functionalization and specifically the installation of CN^- and $COOMe^-$ functional groups have high utility value in organic chemical transformations.[3] The cyanoesterification reaction studied here utilizes 10 mol% of tetrakis(triphenylphosphane)palladium(0) complex as the pre-catalyst. At 110 ºC in toluene after 24 h, the reaction of $Pd(PPh_3)_4$ pre-catalyst with cyanoester reagent and NBE or NBE substrates provided the *exo*-product without observing even traces of the *endo*-isomer.[1] The origin of this strong *exo*-selectivity has yet to be explored.

Beside the *exo*-selectivity, another remarkable feature of the proposed reaction mechanism[1b] (Scheme 1) of the $Pd(PPh_3)_4$ (**1**)-catalyzed cyanoesterification of NBE is the possibility to isolate the oxidative addition product alkoxycarbonylpalladium(II) complex (Pd^{II}(CN)(COOR)$(PPh_3)_2$, **2**). The addition of alkyl cyanoformates (NC–COOR) to complex **1** can take place at room temperature or below 50 ºC in toluene. The resulting *trans* isomer of **2** (**2t2P**, Scheme 2) can be isolated in 89-98% yields.[4]

(Insert Schemes 1 and 2)

The *cis*-isomer of **2** (**2c2P**, Scheme 2) has yet to be successfully isolated. Quite a few of the derivatives of **2t2P** with various alkyl substituents (R = Me, Pr, *i*-Pr, and *t*-Bu) have been structurally characterized by X-ray diffraction analyses.[1a,4] The isolation of **2t2P** at lower temperatures than required for olefin activation is an important feature of the reaction; hence, the origin of the exclusive *exo*-selectivity cannot be related to the oxidative addition step taking place at ambient temperature even in the presence of olefin substrate. Furthermore, the use of

2t2P as a pre-catalyst, showed also a remarkable chemoselectivity. Experimentally, neither ethylene nor cyclopentene gave the desired double functionalized C-C bonds.[1b] The exclusive chemoselectivity for strained cyclic olefins and the exclusive regioselectivity for *exo* preference of the addition suggest two dominantly different reasons that govern product formation. The latter observation suggest that the initial substrate coordination to the 14-electron, coordinatively unsaturated complex or complexes derived from **2t2P** may already induce preference for the *exo*-coordination mode, since after migratory insertion, no isomerization would be possible without a C–H or C–C bond cleavage for converting any *endo*-product into the corresponding *exo*-product.

In order to explore the origin of *exo*-selectivity, we carried out density functional theory-based potential energy surface studies for i) the structure, stability with respect of a ligand dissociation, and isomerization of **2** and ii) NBE olefin substrate coordination (**3**). The detailed study on the oxidative addition step, migratory insertion, and reduction elimination will be discussed in follow up publications. The structural insights gained into this remarkable reaction from completing the above two tasks warrant a detailed and focused theoretical treatment as presented here.

Computational Methods

The electronic structure calculations and consequent potential energy surface mapping were carried out using Gaussian09 Revision C.01.[5] The level of theory was defined by the BHandHLYP hybrid functional[6] and the def2-TZVP basis set[7] for all atoms. The specific combination of density functionals and basis sets was selected for the given study on the basis of an earlier multi-edge X-ray absorption spectroscopic (XAS) study.[8] The independent XAS investigation from the given study defined the experimental ground state electronic structure for low and high-valent chloropalladium complexes and bridging and terminal chloride ligands. The specific knowledge of the composition of the frontier orbitals from experiments allows for the calibration of density functional theory and the definition of basis set saturation limit with respect of metal-ligand bonding. The XAS results suggested that the most reasonable combination of density functional and basis set for Pd^{II} and Pd^{IV} complexes is a hybrid functional that contains at least 50% Hartree-Fock exchange and triple-ζ quality basis set. The latter can be considered as a good approximation of the basis-set saturation limit with respect of electronic structure. In this work, solvent effects of electrostatic origin were treated implicitly *via* a polarizable continuum model (PCM, ε = 2.37, solvent radius = 2.82 Å).[9] The covalent nature of solvent effects was considered by using one or two explicit solvent molecules *via* η^2-toluene coordination to unsaturated, 14-electron Pd^{II} complexes. Scheme 2 summarizes the schematic structures of the complex for **2tPT**, **2tT-O**, **2tT-OMe**, **2t2T**, **2cNT**, and **2cOT**. Given that the toluene molecule may compete with olefin in coordination, the calculated thermochemical properties were corrected by the reaction quotient (+RT ln Q) due to the bulk toluene concentration (c = 9.36 M). In addition, we have also corrected for the difference in the entropic contributions in condensed phase vs. gas phase as proposed by Whitesides (see Supporting Information for the implementation).[10] In the given study the helicity of the PPh_3 ligands were not investigated given the expected small energetic contribution in comparison to the decisive difference among the *exo*- vs. *endo*-coordination modes of the olefin substrate.

Electronic structure analysis was carried out by means of Mulliken population analysis.[11] The orbital compositions were determined by singly occupying an orbital of interest. The resulting atomic spin densities for an unpaired electron were used as the measure percent atomic contributions to a given orbital. Energy decomposition analysis was carried out by means of Kitaura-Morokuma-Ziegler-Rauk[12] as implemented in Amsterdam Density Functional program[13] from single point energy calculations on equilibrium structures at BHandHLYP/TZVP level with COSMO–RS[14] based toluene implicit solvent environment. In order to obtain chemically meaningful energy values for the various contributions to fragment bonding energy, the complexes were broken down to Pd^{2+}, CN^-, $COOMe^-$ ionic fragments and phosphane, toluene, olefin ligands.

Results and Analysis

Geometric and Electronic Structures of trans-Pd(CN)(COOMe)(PPh_3)$_2$

The comparison of the experimental crystal structure and the spectroscopically validated DFT optimized structures of complex **2t2P** is shown in Fig. 1. The root mean square deviations of the [PdP_2C_2] moiety is 0.10 Å, while it only increases to 0.20 Å when the atoms shown in Fig. 1[4,15] are considered (Pd(CN)(COOC)(PC_3)$_2$). With respect to internal coordinates, the root mean square deviations of the highlighted bond lengths and bond angles are 0.05 Å and 3.0º. The largest deviations between the calculated and the experimental internal coordinates were found for the C–N and C–O bonds of the CN^- and the $COOMe^-$ ligands (0.09 and –0.14 Å, respectively); while all other bond length deviations are within 0.05 Å. All the calculated bond angles are within 3º of the experimental values, except the ester C–O–C angle. A closer look at the network of intermolecular interactions of the experimental structure defining the crystal packing forces (the Supporting Information, Fig. S1) provides an explanation for the considerable difference between these experimental and theoretical values. Both CN^- and $COOMe^-$ ligands are involved in multiple aromatic C–H···O/N hydrogen bonds. These are expected to cause distortions in a crystal phase structure relative to the toluene solvated structures, as modeled here.

(Insert Fig. 1)

A detailed electronic structure analysis is warranted here given its implication toward ligand exchange, olefin coordination, and in general the importance of orbital and steric interactions in determining the relative stability of the complexes. Despite the formally straightforward electronic structure that is expected for a 16-electron, yet coordinatively saturated Pd^{II} complex with $4d^8$ electron configuration, **2t2P** displays a remarkably rich electronic structure as manifested by the frontier unoccupied orbitals. The HOMO/LUMO gap is large (7.1 eV), but the LUMOs are close to each other in energy due to the numerous π^* and σ^* orbitals of the ligands as represented by the first 3 eV energy range containing 26 orbitals. The first 15 orbitals are shown in Fig. S2 along with an orbital energy diagram. As expected, the LUMO corresponds to the σ^* orbital between the Pd $4d_{x^2-y^2}$ and the combination of ligand orbitals. It is notable that the P lone pair has a non-negligible π-mixing with the 2p orbitals in the *ipso*-positions of the aromatic ring. The LUMO composition can be described with 15% Pd, 3% CN^-, 12% $COOMe^-$, and 70% PPh_3 contributions. This reflects a highly covalent bonding with remarkably high P→Pd electron donation. The energetically higher lying LUMOs mainly localized on the aromatic rings of the phosphane ligands with varied contributions (up to 2%) from occupied Pd 4d orbitals. These metal contributions can be considered as the measure of Pd→ligand back-donation. LUMO+12, which is still within 1.5 eV of the LUMO started to show the large lobes generally associated with Rydberg orbitals (5s and 5p). Unexpectedly, LUMO+13, which closes a block of LUMOs up to 1.4 eV in energy relative to the LUMO has similar σ^* interaction for C-P bond as shown in the isocontour plot of the LUMO. The orbital composition is 17% Pd $4d_{x^2-y^2}$, 5% CN^-, and 11% $COOMe^-$, and again approximately 70% PPh_3 contributions, but the latter is dominantly aromatic π^*. This is a remarkable electronic structural feature of this complex and shows how important the covalent interactions are in structure and stability of these Pd^{II} complexes.

In addition to the atomic composition and graphical illustrations of the unoccupied frontier orbitals, we also carried out energy decomposition analysis[16] of the metal and ligand interactions according to the Kitaura-Morokuma-Ziegler-Rauk method.[12] Starting from the distorted ligand fragments as in complex **2t2P**, the total fragment bonding energy is 3820 kJ mol^{-1}, which originates from –1414 kJ mol^{-1} steric (Electrostatic + Pauli repulsion), –2338 kJ mol^{-1} orbital relaxation energies, and –67 kJ mol^{-1} solvation energy. The presence of two negatively charged ligands, the polarizable phosphane ligands, as well as the composition of molecular orbitals described above well justifies the large magnitude of these bonding energy contributions. As expected from the covalent bonding picture from the molecular orbital analysis, the orbital interactions are dominating the bonding energy. When we consider the distortion energy of the ligands relative to their fully optimized, but solvated structures, the steric interactions drop to –194 kJ mol^{-1}, but the orbital contribution further increases to 3263 kJ mol^{-1} with negligible solvation energy contribution (–10 kJ mol^{-1}), the total bonding energy remains practically similar in order of magnitude (3533 kJ mol^{-1}). This further emphasizes the importance of covalent bonding. Each ligand undergoes an 8-18 kJ mol^{-1} distortion upon coordinating to the Pd^{II}, which originates from 143, 167, and 744 kJ mol^{-1} steric, but -142, -159, -718 orbital energy contributions for CN^-, PPh_3, and $COOMe^-$, respectively. The large difference between the structure of the free and the coordinated alkoxycarbonyl ligand is notable, as upon binding the carboxylato C–O bond contracts by approximately 0.1 Å, while all the other O containing bonds remain the same within 0.02 Å. This structural change correlates with the change of the electronic structure of formally sp^3 O by involving its out-of-plane lone pair with π-interactions with the Pd 4d orbitals (see LUMO and LUMO+13 in Fig. S2).

Potential energy surface of ligand dissociation and isomerization from 2t2P

In order to evaluate the reactivity of **2t2P**, we carried out a detailed potential energy surface study with respect to formation of the 14-electron complex *trans*-$Pd^{II}(CN)(COOMe)(PPh_3)$, **2tP** after the dissociation of a PPh_3 ligand from **2t2P**. We have evaluated several possible pathways for the isomerization of the CN^- and $COOMe^-$ ligands from *trans* to *cis* position giving complexes **2cOP** and **2cNP**. The 'OP' and 'NP' suffixes indicate *trans*-relationship between the CN^- and the $COOMe^-$ ligands, respectively, and the PPh_3 ligand. The schematic molecular structures for all the intermediates considered in this study are summarized in Scheme 2. Either of the 14-electron *cis*-$Pd^{II}(CN)(COOMe)(PPh_3)$ complex can accept a PPh_3 ligand to complete its coordination environment and form a complex *cis*-$Pd^{II}(CN)(COOMe)(PPh_3)_2$, **2c2P**. Given that we will be exploring the reactivity of the 14-electron complexes toward olefins, we have also considered explicit solvent molecules, since toluene can form η^2-complexes with **2tP**, **2cOP**, or **2cNP**. Fig. 2 summarizes the relative Gibbs free energies of all the considered species toward the activation of **2t2P** for the olefin coordination.

Starting from the most stable and experimentally isolable **2t2P** complex, the initial PPh_3 ligand dissociation requires activation energy of approximately 80 kJ mol^{-1}. This is a reasonable energy for the ligand dissociation at elevated temperatures of 110 ºC as can be judged from established experimental enthalpy change of 129 kJ mol^{-1} for reactions at temperatures ranging 85–119 ºC.[17] The covalent nature of the Pd-P bond has already been discussed in the previous electronic structure analysis section. It is remarkable that the 16-electron toluene complex **2tPT** is practically energetically degenerate to the **2tP** complex and thus indicates that **2tPT** may be formed in solution. The dissociation of the second PPh_3 ligand to give **2t** is energetically prohibitive (+206 kJ mol^{-1}). The coordination of one (isomers **2tT-O** and **2tT-OMe**) or two (**2t2T**) toluene solvent molecule although stabilizes the 12-electron complex

2t; however, it is still out of reach for the given reaction conditions.

It is more relevant to consider the two transition states at 97±1 kJ mol^{-1} labeled **c/t TS** in Fig. 2. These transition states **2cNP_TS** and **2cOP_TS** correspond to the isomerization of **2tP** to the *cis*-isomer with *trans*-CN$^-$/PPh$_3$ ligands (**2cNP**) at 98 kJ mol^{-1} and the isomerization of **2cNP** to the other *cis*-isomer with *trans*-COOMe$^-$/PPh$_3$ (**2cOP**) at 96 kJ mol^{-1}, respectively. For the sake of completeness, we have also located the transition state connecting **2tP** with **2cOP**, but it was found to be much higher (188 kJ mol^{-1}) than any of the above two. This correlates well with the structural analysis above indicating that the COOMe$^-$ undergoes large structural reorganizations upon coordination to the Pd^{II} center due to the possibility of multiple bonding interactions. Upon coordination of a PPh$_3$ ligand to either **2cNP** or **2cOP**, the *cis*-Pd^{II}(CN)(COOMe)(PPh$_3$) complex (**2c2P**) is formed, which is approximately 30 kJ mol^{-1} higher in energy than the *trans* isomer **2t2P**. It is worth noting that considering the explicit solvation, the both *cis*-isomers can coordinate toluene instead of the PPh$_3$ ligand; however, their relative energies shown in Fig. 2 are much higher (110 and 131 kJ mol^{-1} for **2cNT** and **2cOT**, respectively) than the corresponding *trans*-isomer (85 kJ mol^{-1} for **2tPT**). The large relative energy differences indicate that these complexes will not be competitive with olefin substrate coordination.

(Insert Fig. 2)

Fig. 3 compares the immediate coordination environment of the key intermediates from the potential energy surface in Fig. 2. Upon dissociation of a PPh$_3$ ligand from **2t2P** (Fig. 1B), the resulting 14-electron complex **2tP** (Fig. 3A) undergoes a minor structural rearrangement with respect of Pd-ligand bond lengths, with the exception of the Pd-P bond, which contracts by 0.1 Å due to eliminating the *trans* influence of the phosphane ligands. Consequently, the removal of the bulky PPh$_3$ ligand allows for large angular distortion around the Pd centre as the remaining three ligands will take advantage of the vacant coordination site. The changes in bond angles are as large as 10º. The replacement of a PPh$_3$ ligand with a toluene solvent molecule (Fig. 3B) slightly reverses the trend, but judging from the Pd-P distances in **2t2P**, **2tP**, and **2tPT** the toluene is a much poorer donor than PPh$_3$. The toluene coordinates in η^2-fashion at 2.50 Å distance between the Pd^{II} ion and the centroid of the coordinated C=C bond (indicated by a transparent blue sphere in Fig. 3B). The plane of the toluene ring is bent by approximately 20º relative to the perpendicular arrangement to the basal plane defined by [PdCCP].

(Insert Fig. 3)

The optimized structures of the 14-electron, *cis* isomers are shown in Figs. 3C and 3D with remarkable, but not unexpected differences in the inner coordination environment of the Pd^{II} ion. The COOMe$^-$ ligand structure is comparable in both **2cNP** and **2cOP**; however, the Pd-P and Pd-CN distances differ greatly according to the *trans*-influence of the PPh$_3$ and CN$^-$ ligands. In **2cNP**, the Pd-P distance is short (2.37 Å), while the Pd–CN distance is long (2.03 Å), relative to the **2cOP** complex with the corresponding bond lengths of 2.46 Å and 1.95 Å, respectively. Furthermore, the P-Pd-CN bond angle (178º) is only a few degrees off from the ideal linear value in **2cNP**; while the P–Pd–COOMe angle (167º) is similarly distorted as the NC–Pd–COOMe angle (170º) in **2cOP**. The *cis*-isomer for the 16-electron complex **2c2P** in Fig. 3E shows the competition of the ligands for the Pd^{II} central ion, with the longest Pd-P bond (2.50 Å) being *trans* to the COOMe$^-$ ligand; while the other Pd-P bond (2.39 Å) *trans* to the CN$^-$ ligand is comparable to that in **2t2P** (2.38 Å). The steric bulk of the PPh$_3$ ligands in **2c2P** generates so much repulsion that the P-Pd-P bond angle opens up by 10º relative to the ideal perpendicular value. While the complex remains tetragonal, the result of this steric repulsion is the compression of the NC–Pd–COOMe bond angle by approximately 10º.

The molecular structures corresponding to the three possible isomerization transition states for the 14-electron complexes are summarized in Fig. 4. The displacement vectors corresponding to the normal modes with imaginary frequencies (**trans-cisNP** (119*i* cm^{-1}), **cisOP-cisNP** (101*i* cm^{-1}), **trans-cisOP** (256*i* cm^{-1}) are shown in Fig. S3. It is notable that by looking at the structural distortions relative to the 14-electron complexes one can anticipate the nature of the transition state. In Fig. 4A, the Pd–P and Pd–COOMe distances are remarkably short (2.26 and 1.94 Å, respectively), while the Pd-CN distance is quite long (2.17 Å). In addition, the P-Pd-CN and the MeOOC–Pd–CN bond angles are approximately the same within a few degrees. These all together indicate that the CN$^-$ ligand is transitioning between positions corresponding to **2tP** and **2cNP**. In Fig. 4B, the PPh$_3$ ligands becomes partially detached from the Pd^{II} ion, and forms symmetrical angles relative to the other two, stronger coordinating anionic ligands. The latter structural distortions correspond to a transition between **2cNP** and **2cOP**, as also indicated by the normal mode vectors in Fig. S3B. The third transition state has a weakened Pd–COOMe bond, which has the highest energetic penalty, as shown in Fig. 2. In Fig. 4C, the P–Pd–COOMe and the NC–Pd–COOMe angles become equally distorted around 138º, and the Pd–COOMe bond is record long among all the structures presented in Figs. 4 and 5. The transition state structures and their relative energies nicely illustrates the connectedness of the Pd–PPh$_3$ and Pd–CN bonds, while the Pd–COOMe bond is very strong with even multiple bonding character, as presented by the electronic structure of **2t2P**.

There is a notable inverted trend for the stability of *cis*- and *trans*-isomers for the 16- (**2t2P** *versus* **2c2P**) and the 14-electron (**2cNP/2cOP** *versus* **2tP**) complexes, which requires further analysis. Therefore, we have carried out detailed energy decomposition analysis for all the relevant intermediates presented in Fig. 2 and structurally analysed in Figs. 4 and 5. The different relative energies can be related to the relative importance of covalent interactions *versus* the steric repulsion. This initial hypothesis was generated on the basis of L-Pd-L

bond angles in **2c2P** showing greater deviation from the ideal 90/180º tetragonal coordination environment than those in **2t2P**.

(Insert Figs. 4 and 5)

The results of energy decomposition analysis are summarized in Table 1. Notably, the numbers in Table 1 for **2t2P** are different than those used for the energy decomposition analysis above, because in Table 1 the penalty of fragment reorganization was already included as all numbers were defined relative to the relaxed, equilibrium geometries of every ligand and the S =1 spin state of the isolated Pd^{2+} ion. Table 1 nicely supports numerically the hypothesis generated on the basis of structural distortions. In going from **2t2P** to **2c2P**, the steric energy contributions go from negative to positive; respectively. Although the orbital stabilization increases in the same order (-88 kJ mol^{-1} for 4 ligands); however it cannot make up for steric repulsion increase (+381 kJ mol^{-1}) and thus the total bonding energy will be less favourable for the *cis*-isomer by 24 kJ mol^{-1}. The steric energy differences between the 14-electron complexes **2tP** and **2cNP** follow a similar trend (+270 kJ mol^{-1}) as for **2t2P** to **2c2P**; but now the ligands allowed to come in closer to the metal due to the lack of the bulky PPh_3 ligand, have better overlap, and thus contribute to a larger covalent orbital stabilization for **2cNP** than for **2tP** (-95 kJ mol^{-1} for 3 ligands). The reverse trend in the bonding energetically favours **2cNP** versus **2tP** by 19 kJ mol^{-1}. The finer structural differences between the two 14-electron *cis* isomers are also elaborated by the energy decomposition analysis. Placing the bulkier $COOMe^-$ ligand *trans* to the PPh_3 ligand in **2cOP** results in reduced steric repulsion (-139 kJ mol^{-1}), but the stronger *trans* influence of the $COOMe^-$ and the PPh_3 ligands also reduces the orbital stabilization (+143 kJ mol^{-1}) and overall contribute to weaker bonding for **2cOP** *versus* **2cNP**.

(Insert Table 1)

The larger orbital energy stabilization in **2c2P** (-3612 kJ mol^{-1}) relative to **2t2P** (-3263 kJ mol^{-1}) has electronic structural origins. Fig. S4 summarizes the relevant orbitals for the first 15 LUMOs in **2c2P** similarly to Fig. S2 for **2c2t**. A cursory comparison of the LUMOs and their orbital energy levels for **2c2P** and **2t2P** already reveals the much more pronounced mixing of metal and ligand fragment orbitals in the *cis*-isomer. This is directly responsible for the larger orbital stabilization, as shown in Table 1. Both the LUMO and LUMO+1 has approximately 9% Pd $4d_{x^2-y^2}$ orbital contribution with a comparable $COOMe^-$ and only a few percent of CN^- orbital contributions, while the rest is all coming from the PPh_3 ligands. LUMO+3, 4, 6, 8, and 10 have much larger Pd 4d orbital character and thus larger back-donation than in the *trans*-isomer. However, similarly to **2t2P**, LUMO+13 shows the typical orbital lobes expected for a square planar Pd^{II} complex with 18% Pd, 5% CN^-, 11% $COOMe^-$, and the rest is from PPh_3 ligand. It is then understandable why and how the interplay of steric and orbital interactions, the mixing of ligand/metal and ligand/ligand orbitals are important for the origin of exclusive *exo*-selectivity in the cyanoesterification reaction of norbornene.

Olefin Substrate (Norbornene) Coordination to give Complexes 3

The most striking feature of the potential energy surface of the olefin coordination to the various isomers of $[Pd^{II}(CN)(COOMe)(PPh_3)]$ complexes in Fig. 5 is the unambiguous energetic separation of the *exo*-and *endo*-coordinated NBE complexes. The highest energy conformer of *exo*-**3cOP** was calculated to be 8 kJ mol^{-1} lower in energy than the lowest energy conformer of *endo*-**3tP-N**. These computational results clearly predict a strong preference for *exo*-coordination of the olefin substrate, which then results in the experimentally observed *exo*-selectivity of the cyanoesterification reaction of NBE using $Pd(PPh_3)_4$ pre-catalyst. As presented above for the preference between *cis* and *trans* isomers for the 16- *versus* 14-electron complexes, upon the norbornene coordination the *trans* isomers become lower in energy for both *exo*- and *endo*-NBE coordination modes. For the *exo*-coordination mode, the most stable complex *exo*-**3tP-O** has comparable Gibbs free energy to the lowest 14-electron complex **2cNP**. Using data shown in Fig. S5, which displays the enthalpy of an NBE coordination *versus* a reaction coordinate, we can estimate the binding energy of NBE relative to **2cNP** to be -29, -17, -8, and +2 kJ mol^{-1} for *exo*-**3tP-O**, *exo*-**3tP-N**, *exo*-**3cNP**, and *exo*-**3cOP**, respectively. The comparable relative binding enthalpy values are +9, +11, +13, and +31 kJ mol^{-1} for *endo*-**3tP-N**, *endo*-**3tP-O**, *endo*-**3cNP**, and *endo*-**3cOP**, respectively. The relative binding free energies of the most stable *exo*-complexes, *exo*-**3tP-N** and *exo*-**3tP-O** to **2cNP** are +37 and +37 kJ mol^{-1}, respectively.

(Insert Fig. 5)

The origin of large energetic difference between the *endo*- and *exo*-coordination of NBE was further investigated by comparing their molecular structures (Figs. 6 and 7) and energy decomposition of the metal-ligand bonding energies (Table 2). The major difference among the *exo*-and *endo*-coordination isomers of NBE complexes is the distance between the Pd^{II} ion and the C=C bond. The shorter and thus stronger Pd^{II}–olefin π-bonds correspond exclusively to the *exo*-coordination. As a limited conformation analysis of the olefin orientation relative to the Pd-ligands, we considered two characteristic conformations, when the NBE methylene bridge in the *exo*-and the distal C–C bond in the *endo*-coordination are eclipsed with the CN^- or $COOMe^-$ ligands in a *cis*-position to NBE. In all cases the pre-set conformation has remained with the exception of *exo*-**3tP-O** (Fig. 6A), where the olefin rotated to be parallel with the *trans* MeOOC–Pd–CN bonds and the proximal H atom of the methylene bridge formed an agostic H–bond with Pd via the doubly occupied $4d_{z^2}$ orbital. This interaction leads to the

most stable olefin complex with the shortest Pd···C=C bond centroid distance of 2.33 Å. Formally, a 90º rotation along the Pd···C=C bond centroid axis will result in *exo*-**3tP-N** (Fig. 6B), which now have a considerably elongated Pd···C=C bond centroid distance of 2.41 Å; however, with a much shorter methylene bridge H···C(CN^-) distance of 2.39 Å. As discussed above, the strong *trans*-influence of the $COOMe^-$ ligand results in the longest and thus the weakest Pd-olefin π-bond in *exo*-**3cNP** (Fig. 6C). However, when the olefin is *trans* to the CN^- ligand, its distance to Pd drastically reduced as can be seen for *exo*-**3cOP** (Fig. 6D). The structural differences of the various isomers are well paralleled by the energy differences in Fig. 5 (Gibbs free energy) and Fig. S5 (enthalpy).

(Insert Figs. 6 and 7)

The molecular structures of all the *endo*-NBE complexes in Fig. 7, clearly indicate the unfavourable coordination of the olefin due to the steep angles between the plane of the C=C bond and the Pd^{II}···olefin bond centroid axis. The kinked coordination of NBE reduces the efficiency of the olefin→Pd electron donation in comparison to those in the *exo*-isomers. The interaction between the H atoms at the distal C–C bond of NBE and the CN^- or $COOMe^-$ ligands slightly contributes to the stability of the complexes, but not enough degree to affect the preference for the *exo*-coordination. Interestingly, the shortest Pd···C=C bond centroid distance was found for the least stable complex (*endo*-**3cOP**, Fig. 7D), which is a difference to the *exo*-isomers. Strong *trans*-influence of the $COOMe^-$ ligand is also visible for *endo*-**3cNP** (Fig. 7C) by elongating the Pd···C=C bond centroid distance to more than 2.8 Å. Given that the two distal H atoms of the NBE ligand in the *trans* isomers can only form weak agostic interactions with the Pd^{II} ion; both eclipsed isomers were localized as stationary structures (*endo*-**3tP-N,O**, Figs. 7A and B) with comparably short Pd···C=C bond centroid distance (2.61 and 2.59 Å, respectively). Their relative Gibbs free energy (Fig. 5) and enthalpy (Fig. S5) values are practically identical.

The energy decomposition analyses of overall complex formation (left side of Table 2) and the NBE dissociation energy (right side of Table 2) further elaborate the structural and energetic differences described above. Comparison of the orbital and steric contributions to the bonding energy for the complex formation suggests the importance of covalent orbital interactions, similarly to the complexes prior to the olefin coordination. With the exceptions of *exo*-**3tP-O** and *exo*-**3tP-N**, the steric and solvation contributions to the total binding energy can be neglected relative to the orbital relaxation energy between the separate free ligands and Pd^{2+} ion and their corresponding complexes. The large negative steric contribution in the latter complexes indicates the lack of a steric repulsion for the *exo*-coordination of NBE to the $Pd^{II}(PPh_3)(CN)(COOMe)$ complexes with either the CN^- or the $COOMe^-$ ligands being *trans* to the PPh_3 ligand.

(Insert Table 2)

The comparison of the NBE dissociation energies relative to the free, relaxed NBE ligand and the corresponding 14-electron Pd^{II} complexes shows a notable trend. The strongest NBE binding is calculated for *exo*-**3cOP** with 133 kJ mol^{-1} bonding energy when NBE is *trans* to the weakest donor ligand (CN^-) and form C-H···O hydrogen bonding interactions at 2.34 Å with the π-bonds of the $COOMe^-$ ligand (Fig. 6D). Considering the bonding energy of all the ligands, the same complex will be the least stable (-3438 kJ mol^{-1} in Table 2). A similar set of interactions explains the exceptionally high bonding energy for *endo*-**3cOP** as an anomaly among the *endo*-isomers. The weakest NBE bonding in *endo*-**3cNP** (41 kJ mol^{-1}) correlates well with the longest Pd···C=C bond centroid distance of 2.81 Å among all the studied NBE complexes (Fig. 7C).

Discussions

A detailed structural and energetic analyses of the initial olefin coordination step after the oxidative addition step revealed the origin of exclusive *exo*-selectivity in the cyanoesterification reaction of norbornene catalysed by $Pd(PPh_3)_4$. The given study was started from the last intermediates of the oxidative addition steps. The justification of the *in media res* investigation of the molecular mechanism of the reaction is provided by the experimental observation that room-temperature reaction of the pre-catalyst and the cyanoformate substrate allows for the isolation of the oxidative addition product **2t2P**. We evaluated computationally the possibility of formation of the **2c2P** isomer by warming up the solution to overcome the barrier for isomerization reaction upon dissociation of a PPh_3 ligand. The potential energy surface mapping suggested that the key step in the isomerization is the dissociation of the PPh_3 ligand (ΔG = +81 kJ mol^{-1}), which can be aided by the coordination of the solvent toluene. From the coordinatively unsaturated, 14-electron complex **2tP**, the isomerization transition state is only 17 kJ mol^{-1} higher, which allows this complex to convert into the most stable 14-electron *cis*-isomer **2cNP** (+44 kJ mol^{-1}). Through a 52 kJ mol^{-1} barrier, **2cNP** can isomerize to the other *cis*-isomer **2cOP**, which is higher in energy by 20 kJ mol^{-1}. Due to the steric bulk of the coordinated PPh_3 ligand, none of the *cis*-isomer showed a preference for solvent toluene coordination. However, the dissociated PPh_3 ligand can coordinate to **2cNP** giving **2c2P** coordinatively saturated complex, which is 31 kJ mol^{-1} higher energy than the preparatively accessible **2t2P**, but it is 13 kJ mol^{-1} more stable than the lowest energy 14-electron complex, **2cNP**.

Norbornene coordination and further activation toward the installation of the CN^- and $COOR^-$ groups over the C=C bond requires elevated temperatures, such as 110 ºC. From the above analysis of the isomerization of **2t2P** to **2c2P**, we can assume that some non-negligible percentage of the coordinatively unsaturated complexes would be present at elevated reaction temperature relative to the oxidative addition step. From the potential energy surface map in Fig. 5, the **2cNP** complex will likely be the dominant coordinatively unsaturated species,

which is activated toward the coordination of NBE to the Pd centre. Formation of the *exo*-**2cNP** complex is preferred by 17 kJ mol^{-1} over the *endo*-isomer. Relevantly to the main goal of the given study, there is a clear energetic preference for the *exo*-isomer when considering all the possible NBE complexes. An energy range formed by the possible *exo*-isomers does not even overlap with the energy range of the *endo*-isomers. The calculated differences in Gibbs free energy, as well as the enthalpy of the norbornene coordination clearly demonstrate the exclusive *exo*-selectivity of the norbornene cyanoesterification reaction.

The origin of *exo*-selectivity thus must lie in the nature of the NBE coordination to 14-electron $Pd^{II}(CN)(COOMe)(PPh_3)$ complex. By comparing the NBE π-complex structures of both *exo*- and *endo*-coordination modes an apparent difference can be noted. In order to form a stable π-complex, the acceptor Pd 4d orbital needs to be perpendicular to the plane of the highest occupied π–orbital. This automatically maximizes the possibility for π-back-donation if the metal is electron-rich enough. For the *endo*-isomers this angle was calculated to be approximately 133º, while for the *exo*-isomers it is 11º closer to the ideal 90º value. These values were obtained by measuring the angle formed by the Pd, C=C bond centroid, and C–C=C–C plane centroid. The distortion of 11º corresponds to approximately 17-30 kJ mol^{-1} stabilization with respect of Gibbs free energy.

The *exo*-face of the LUMO points toward a five-membered ring of NBE; while the *endo*-face toward the six-membered ring. The methylene bridge C and proximal H atoms in the *exo*-coordination mode are 2.24 and 2.56 Å away from the coordinated C=C bond centroid; respectively, while these distances are 2.56 and 2.82 Å away in the *endo*-coordination mode for the C and the H atoms of the ethylene bridge. These metric differences would indicate that there is "more" room available for the coordination in the *endo*-isomer; however, the governing factor for the olefin coordination is the orientation of the lobes of the π-LUMO. In the six-membered ring, the π-complex cannot approach the ideal 90º for maximal Pd 4d, π-ligand orbital overlap, because the centroid of the ethylene bridge of NBE would collide with the *cis* ligand on the metal. Contrary, in the *exo*-isomer the methylene bridge has a smaller steric bulk in addition to the presence of C–H bonds that can form agostic H-bond with the metal or with the *cis*-ligand and thus allowing the Pd 4d, C=C centroid, C–C=C–C centroid angle to get considerably closer to the ideal 90º than in the *endo*-isomer, thus for a more stable olefin π-complex.

Conclusions

The use of spectroscopically calibrated, hybrid density functional theory allowed us to provide key insights into the effect of different reaction conditions on the oxidative addition products and their isomerization. We have identified key transition states that connect the late steps of oxidative addition. These steps are also the starting point for olefin π-complex formation for the transfer of the cyano and ester groups from the Pd complex to the C=C bond. We have shown that even without the complete molecular description of the reaction mechanism of the Pd-catalysed cyanoesterification of norbornene, we can define the key structural factors that govern the exclusive *exo*-selectivity. The key recognition of the relative stability of *exo*- versus *endo*-isomers originates from the composition and structure of norbornene substrate itself. The smaller steric bulk of the bridging methylene group and the possibility for the C–H bond of the methylene bridge to form weak, but non-negligible H-bonding interaction provide a 17-30 kJ mol-1 preference for the *exo*-isomer. In the *endo*-isomer, the bulkier ethylene bridge of norbornene bends the olefin π-donor orbital away from the ideal perpendicular orientation by 11º more relative to the *exo*-isomer. Furthermore, the cis-ligands of Pd to norbornene are between the two proximal C–H bonds, which practically eliminate the possibility for the formation of any stabilizing C–H···acceptor atom/group H–bonding interaction. Consequently the difference in the six- versus the fix-membered ring faces of NBE corresponding to the *endo*- versus *exo*-coordination, propagates through the reaction mechanism; however, the energetic preference of *exo*-isomer is large enough for the selectivity to manifest already at the initial substrate binding step. The entire mechanism of the cyanoesterification reaction will be a subject of our forthcoming investigations.

Acknowledgements

This work was supported by Grant-in-Aid for Scientific Research on Innovative Areas "Molecular Activation Directed toward Straightforward Synthesis", No. 23105507 from MEXT to S.M. and a Grant-in-Aid for Scientific Research (KAKENHI) (No. 24550119) from JSPS to Y.N. The generous allotment of computation time from the Research Center for Computational Science (RCCS), the National Institutes of Natural Sciences, Japan, is also gratefully acknowledged. R.K.S. is acknowledges the sabbatical leave from Montana State University.

Notes and references

[a] Division of Chemistry and Biochemistry, Graduate School of Natural Science and Technology, Okayama University, 3-1-1 Tsushimanaka, Kita-ku, Okayama 700-8530, Japan. E-mail: ynishiha@okayama-u.ac.jp
[b] Department of Chemistry and Biochemistry, Montana State University, Bozeman MT, 59717, USA (current address: Department of Analytical Chemistry, University of Pannonia, Veszprem, 8200, Hungary).
[c] Faculty of Science, Ibaraki University, 2-1-1 Bunkyo, Mito 310-8512, Japan. E-mail: smori@mx.ibaraki.ac.jp
[d] Japan Science and Technology Agency, ACT-C, 4-1-8 Honcho, Kawaguchi, Saitama 332-0012, Japan

† Electronic Supplementary Information (ESI) available: [Corrections of translational entropy from Ref 10, Figs. S1-S5 and Cartesian coordinates in XYZ format, and non-truncated molecular structures for all computational models. This material is available free of charge via the Internet at http://pubs.acs.org. Further supporting information with formatted Gaussian checkpoint files, molecular orbital contour maps, computational output files are provided at

http://computational.chemistry.montana.edu/SI.]. See DOI: 10.1039/b000000x/

1 (a) Y. Nishihara, Y. Inoue, M. Itazaki and K. Takagi, *Org. Lett.,* 2005, **7,** 2639–2641; (b) Y. Nishihara, Y. Inoue, S. Izawa, M. Miyasaka, K. Tanemura, K. Nakajima and K. Takagi, *Tetrahedron,* 2006, **62**, 9872–9882.

2 (a) H. Nakazawa, T. Kawasaki, K. Miyoshi, C. H. Suresh and N. Koga, *Organometallics,* 2004, **23**, 117–126; (b) M. Itazaki and H. Nakazawa, *Chem. Lett.,* 2005, **34**, 1054–1055; (c) H. Nakazawa, K. Kamata and M. Itazaki, *Chem. Commun.,* 2005, 4004–4006; (d) H. Nakazawa, M. Itazaki, K. Kamata and K. Ueda, *Chem. Asian J.,* 2007, **2**, 882–888.

3 (a) Y. Nakao, Y. Hirata and T. Hiyama, *J. Am. Chem. Soc.,* 2006, **128**, 7420–7421; (b) Y.Hirata, T. Inui, Y. Nakao and T. Hiyama, *J. Am. Chem. Soc.,* 2009, **131**, 6624–6631; (c) Y. Hirata, A. Yada, E. Morita, Y. Nakao, T. Hiyama, M. Ohashi and S. Ogoshi, *J. Am. Chem. Soc.,* 2010, **132**, 10070–10077.

4 Y. Nishihara, M. Miyasaka, Y. Inoue, T. Yamaguchi, M. Kojima and K. Takagi, *Organometallics,* 2007, **26**, 4054–4060.

5 M. J. Frisch, G. W. Trucks, H. B. Schlegel, G. E. Scuseria, M. A. Robb, J. R. Cheeseman, G. Scalmani, V. Barone, B. Mennucci, G. A. Petersson, H. Nakatsuji, M. Caricato, X. Li, H. P. Hratchian, A. F. Izmaylov, J. Bloino, G. Zheng, J. L. Sonnenberg, M. Hada, M. Ehara, K. Toyota, R. Fukuda, J. Hasegawa, M. Ishida, T. Nakajima, Y. Honda, O. Kitao, H. Nakai, T. Vreven, J. A., Jr. Montgomery, J. E. Peralta, F. Ogliaro, M. Bearpark, J. J. Heyd, E. Brothers, K. N. Kudin, V. N. Staroverov, R. Kobayashi, J. Normand, K. Raghavachari, A. Rendell, J. C. Burant, S. S. Iyengar, J. Tomasi, M. Cossi, N. Rega, N. J. Millam, M. Klene, J. E. Knox, J. B. Cross, V. Bakken, C. Adamo, J. Jaramillo, R. Gomperts, R. E. Stratmann, O. Yazyev, A. J. Austin, R. Cammi, C. Pomelli, J. W. Ochterski, R. L. Martin, K. Morokuma, V. G. Zakrzewski, G. A. Voth, P. Salvador, J. J. Dannenberg, S. Dapprich, A. D. Daniels, Ö. Farkas, J. B. Foresman, J. V. Ortiz, J. Cioslowski and D. J. Fox, *Gaussian 09, Revision C.01*; Gaussian, Inc.: Wallingford, CT, U.S.A., 2009.

6 (a) A. D. Becke, *J. Chem. Phys.,* 1993, **98**, 1372-1377; (b) C. Lee, W. Yang and R. G. Parr, *Phys. Rev. B,* 1988, **37**, 785–789.

7 F. Weigend and R. Ahlrichs, *Phys. Chem. Chem. Phys.,* 2005, **7,** 3297–3305.

8 R. B. Boysen and R. K. Szilagyi, *Inorg. Chem. Acta,* 2008, **361**, 1047–1058.

9 (a) S. Miertuš, E. Scrocco and J. Tomasi, *J. Chem. Phys.,* 1981, **5**, 117–129; (b) J. Tomasi, B. Mennucci and R. Cammi, *Chem. Rev.,* 2005, **105**, 2999–3093.

10 (a) M. Mammen, E. I. Shakhnovich, J. M. Deutch and G. M. Whitesides, *J. Org. Chem.,* 1998, **63**, 3821–3830; (b) A. Ishikawa, Y. Nakao, H. Sato and S. Sakaki, *Inorg. Chem.,* 2009, **48**, 8154–8163.

11 R. S. Mulliken, *J. Chem. Phys.* 1955, **23**, 1833–1840.

12 (a) K. Kitaura and K. Morokuma, *Int. J. Quantum Chem.,* 1976, **10**, 325–340; (b) T. Ziegler and A. Rauk, *Inorg. Chem.,* 1979, **18**, 1558–1565.

13 G. te Velde, F. M. Bickelhaupt, S. J. A. van Gisbergen, C. Fonseca Guerra, E. J. Baerends, J. G. Snijders and T. Ziegler, Chemistry with ADF. *J. Comput. Chem.* 2001, **22**, 931; E. J. Baerends, T. Ziegler, J. Autschbach, D. Bashford, A. Bérces, F. M. Bickelhaupt, C. Bo, P. M. Boerrigter, L. Cavallo, D. P. Chong, L. Deng, R. M. Dickson, D. E. Ellis, M. van Faassen, L. Fan, T. H. Fischer, C. Fonseca Guerra, M. Franchini, A. Ghysels, A. Giammona, S. J. A. van Gisbergen, A. W. Götz, J. A. Groeneveld, O. V. Gritsenko, M. Grüning, S. Gusarov, F. E. Harris, P. van den Hoek, C. R. Jacob, H. Jacobsen, L. Jensen, J. W. Kaminski, G. van Kessel, F. Kootstra, A. Kovalenko, M. V. Krykunov, E. van Lenthe, D. A. McCormack, A. Michalak, M. Mitoraj, S. M. Morton, J. Neugebauer, V. P. Nicu, L. Noodleman, V. P. Osinga, S. Patchkovskii, M. Pavanello, P. H. T. Philipsen, D. Post, C. C. Pye, W. Ravenek, J. I. Rodríguez, P. Ros, P. R. T. Schipper, G. Schreckenbach, J. S. Seldenthuis, M. Seth, J. G. Snijders, M. Solà, M. Swart, D. Swerhone, G. te Velde, P. Vernooijs, L. Versluis, L. Visscher, O. Visser, F. Wang, T. A. Wesolowski, E. M. van Wezenbeek, G. Wiesenekker, S. K. Wolff, T. K. Woo and A. L. Yakovlev, *Amsterdam Density Functional 2013*, SCM, Theoretical Chemistry: Vrije Universiteit, Amsterdam, The Netherlands, 2013.

14 (a) A. Klamt, *J. Phys. Chem.,* 1995, **99**, 2224–2235; (b) A. Klamt, V. Jonas, T. Bürger and J. C. Lohrenz, *J. Phys. Chem. A.,* 1998, **102**, 5074–5085.

15 F. H. Allen, *Acta Crystallograph.,* 2002, **B58**, 380–388.

16 F. M. Bickelhaupt and E. J. Baerends, Kohn-Sham Density Functional Theory: Predicting and Understanding Chemistry. In *Reviews in Computational Chemistry*, Lipkowitz, K. B.; Boyd, D. B., Eds. Wiley-VCH: New York, 2000; Vol. 15, pp 1–86.

17 J. E. Marcone and K. G. Moloy, *J. Am. Chem. Soc.,* 1998, **120**, 8527–8528.

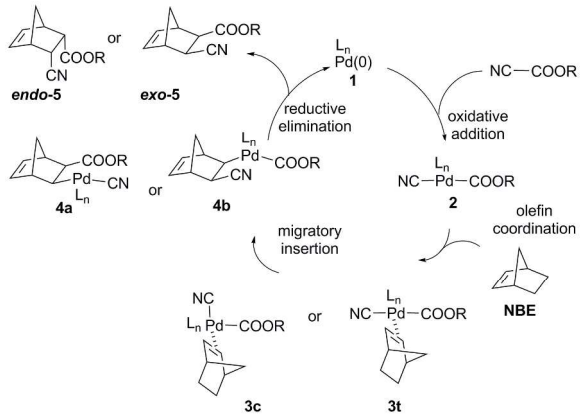

Scheme 1 Schematic reaction mechanism for norbornene cyanoesterification by palladium(0) catalyst as proposed in Ref. 1b.

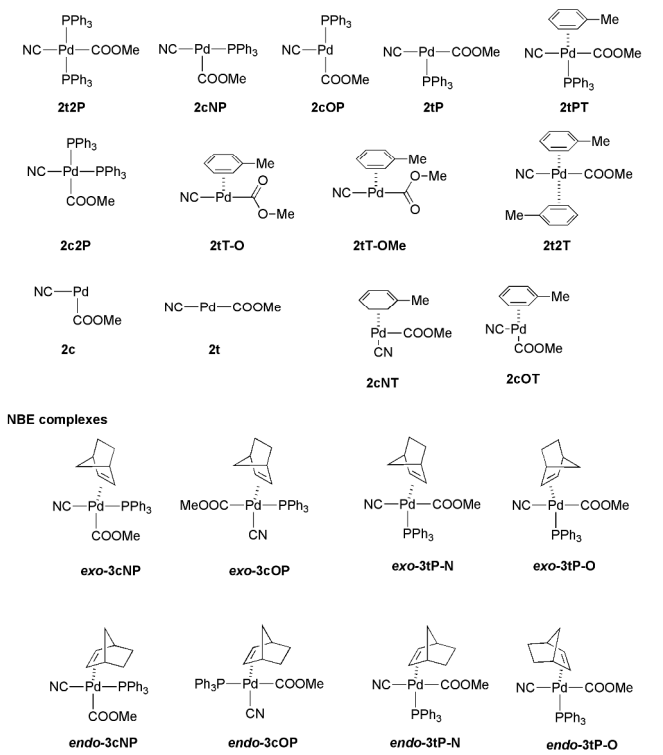

Scheme 2 Schematic representation of intermediates considered in the given study.

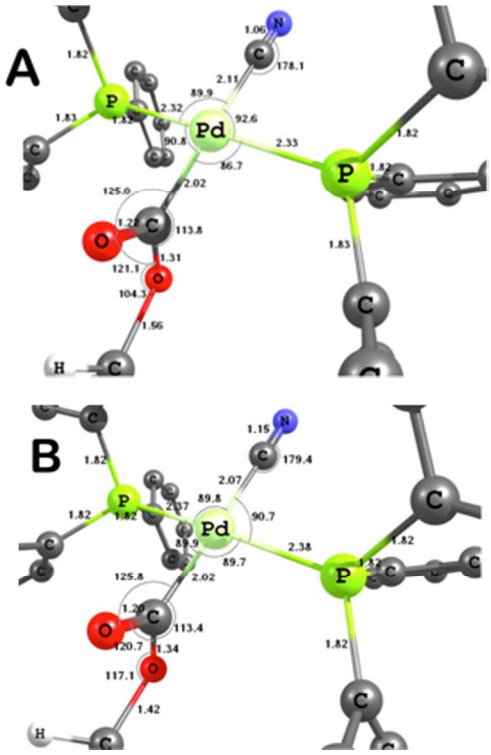

Fig. 1 Comparison of experimental crystal structure (A, CCDB code: DAPRES[4]) and BHandHLYP/def2TZVP/PCM(toluene) calculated structure (B) of **2t2P**. Selected bond lengths and angles are given in Å and degrees. Aromatic H atoms were omitted for clarity and the structures were truncated to emphasize the coordination environment of the central palladium(II) ion.

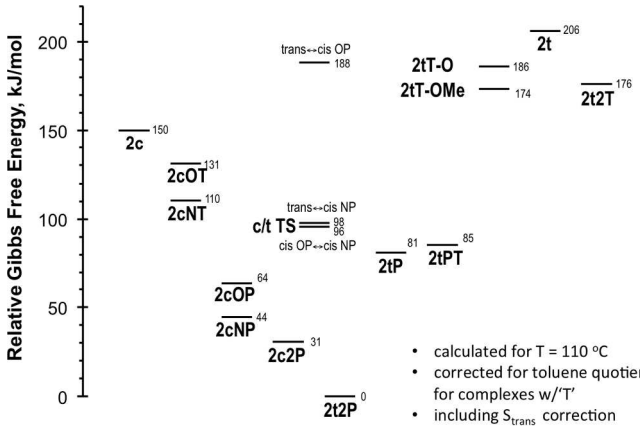

Fig. 2 Corrected Gibbs free energy surface of activation of **2t2P** toward olefin coordination with modification to the solution phase entropy, consideration of the thermodynamic driving force from bulk toluene solvent, for reaction temperature of 110 °C at the BHandHLYP/def2TZVP/PCM(toluene) level.

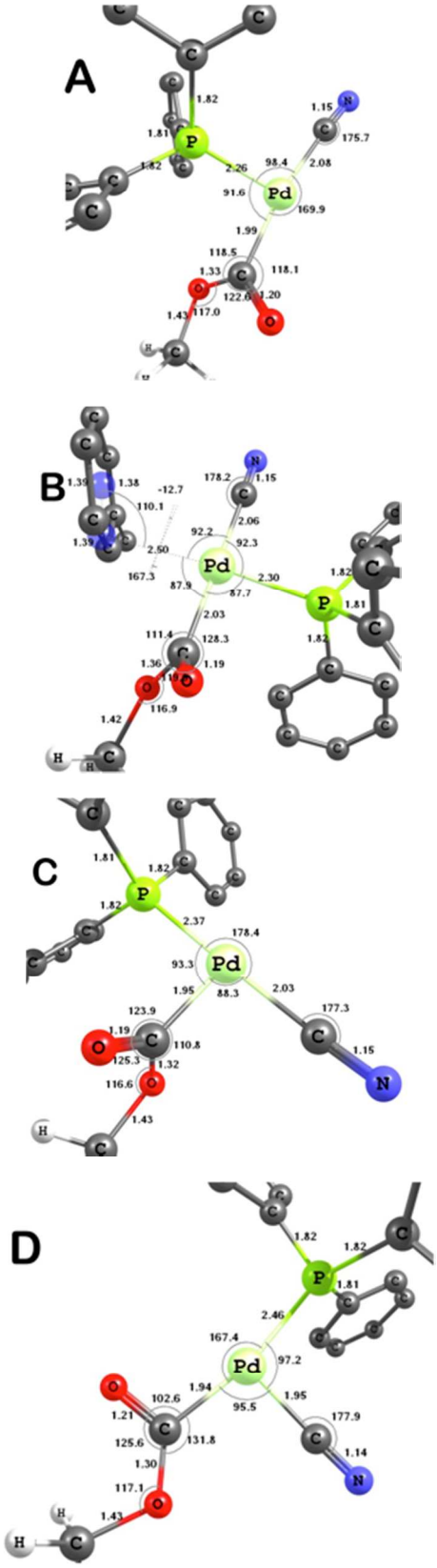

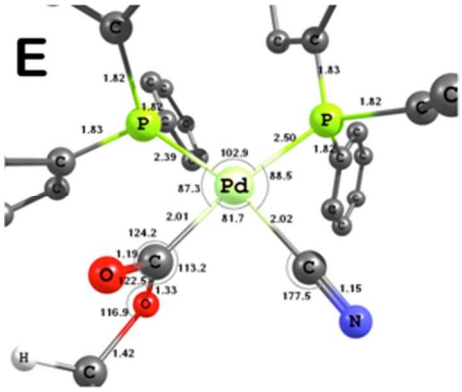

Fig. 3 Calculated molecular structures at the BHandHLYP/def2TZVP/PCM(toluene) level for complexes **2tP** (A), **2tPT** (B), **2cNP** (C), **2cOP** (D), and **2c2P** (E). Selected bond lengths and angles are given in Å and degrees. Aromatic H atoms were omitted for clarity and the structures were truncated to emphasize the coordination environment of the central palladium(II) ion.

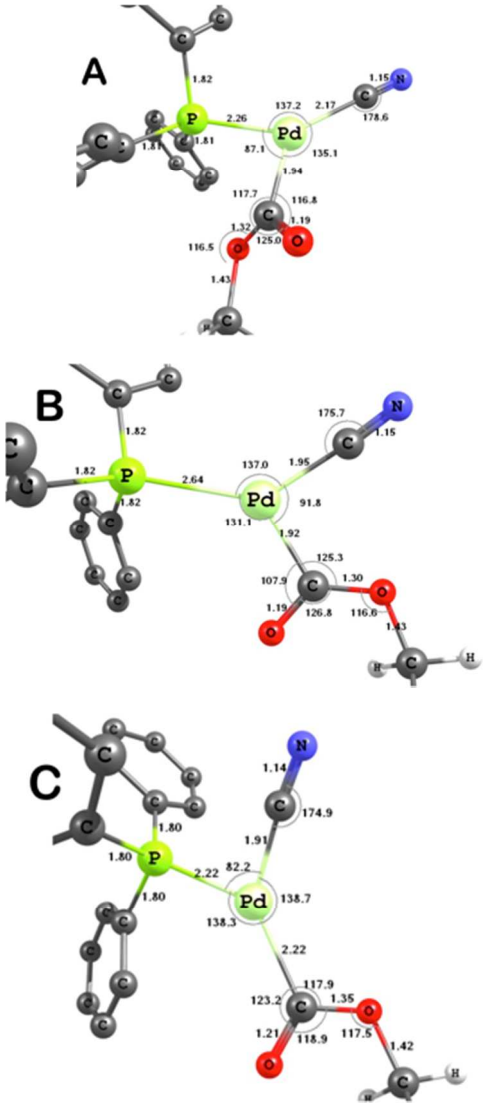

Fig. 4 Molecular structures of isomerization transition states at the BHandHLYP/def2TZVP/PCM(toluene) level for going between **2tP** and **2cNP** (A), between **2cNP** and **2cOP** (B), and between **2tP** and **2cOP** (C). Selected bond lengths and angles are given in Å and degrees. Aromatic H atoms were omitted for clarity and the structures were truncated to emphasize the coordination environment of the central palladium(II) ion. The displacement vectors indicating the change in atomic positions at a given transition state are shown in Fig. S3.

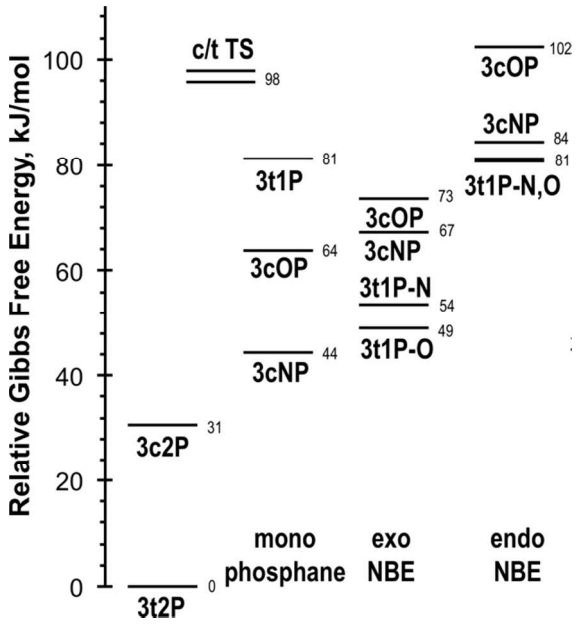

Fig. 5 Relative Gibbs free energy surface of norbornene complexes (**3**) of the 14-electron palladium(II) complexes (**2**) calculated at the BHandHLYP/def2TZVP/PCM(toluene) level ('N', and 'O' suffixes refer to the position of the norbornene methylene bridge *versus* CN^-, and $COOMe^-$ ligands.

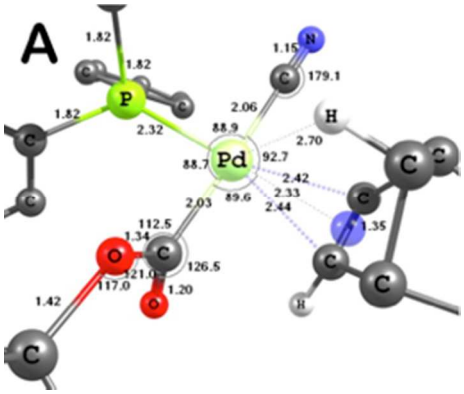

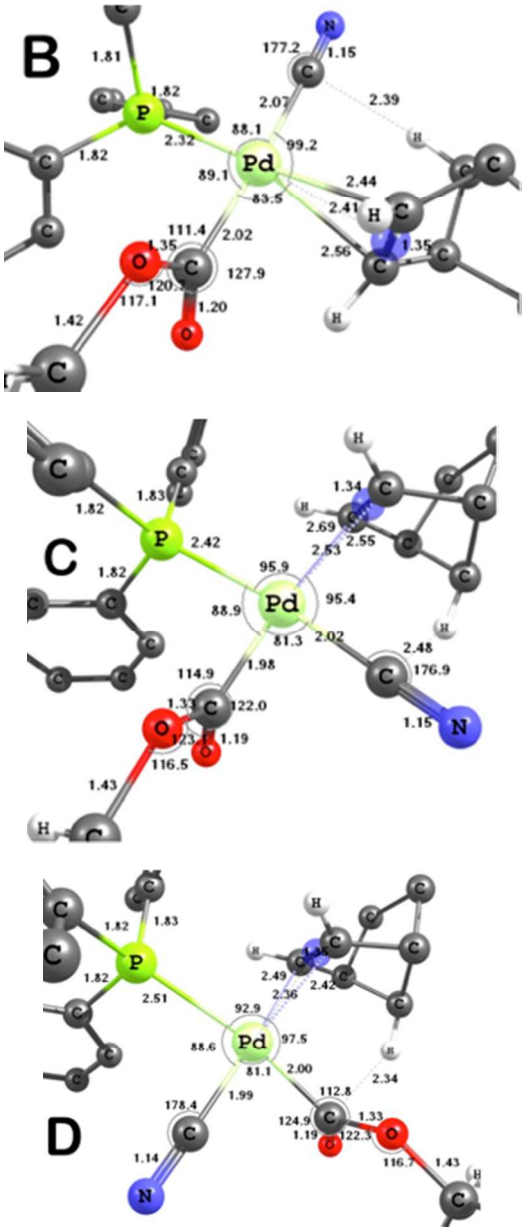

Fig. 6 Molecular structures of *exo*-coordination isomers of NBE to $Pd^{II}(CN)(COOMe)(PPh_3)$ (**2**) (A: *exo*-**3tP-O**, B: *exo*-**3tP-N**, C: *exo*-**3cNP**, A: *exo*-**3cOP**) calculated at the BHandHLYP/def2TZVP/ PCM(toluene) level. Selected bond lengths and angles are given in Å and degrees. Aromatic H atoms were omitted for clarity and the structures were truncated to emphasize the coordination environment of the central palladium(II) ion.

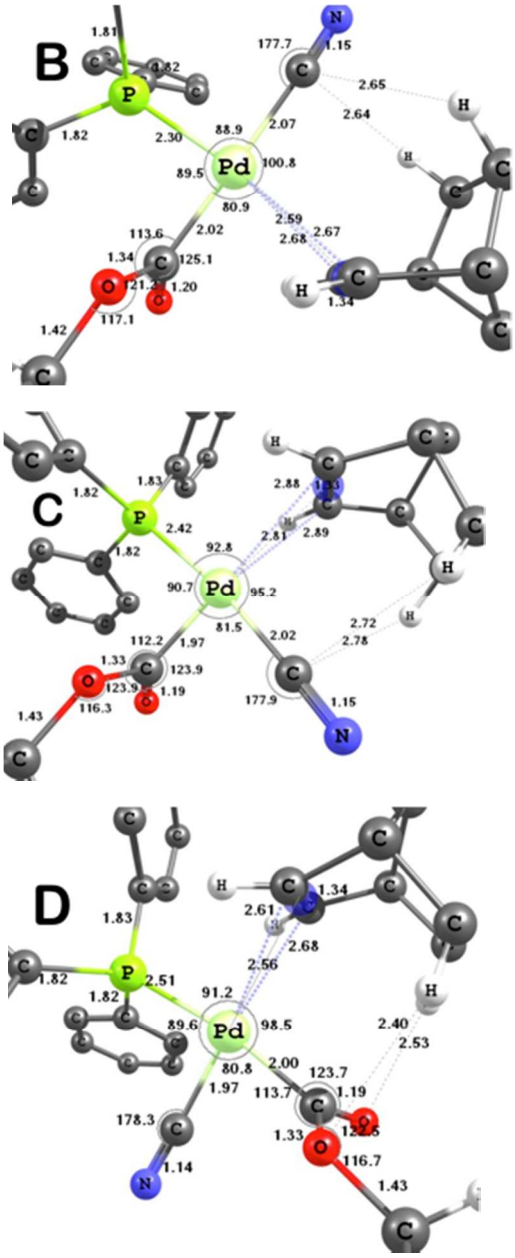

Fig. 7 Molecular structures of *endo*-coordination isomers of NBE to $Pd^{II}(CN)(COOMe)(PPh_3)$ (**2**) (A: *endo*-**3tP-O**, B: *endo*-**3tP-N**, C: *endo*-**3cNP**, A: *endo*-**3cOP**) calculated at the BHandHLYP/def2TZVP/ PCM(toluene) level. Selected bond lengths and angles are given in Å and degrees. Aromatic H atoms were omitted for clarity and the structures were truncated to emphasize the coordination environment of the central palladium(II) ion.

Table 1 The results of Kitaura-Morokuma-Ziegler-Rauk energy decomposition analysis[12,13] in kJ mol^{-1} for key 16- and 14-electron complexes related to the activation of the oxidative addition product $Pd^{II}(CN)(COOMe)(PPh_3)_2$ for olefin coordination (steric energy is the sum of electrostatic and Pauli repulsion terms, orbital energy is the sum of kinetic, Coulomb, and exchange/correlation terms using BHandHLYP functional, bonding is the sum of steric, orbital, and solvation energies).

Complex	Steric	Orbital	Solvation	Bonding
2t2P	-194	-3263	-77	-3533
2c2P	188	-3612	-85	-3509
c/t difference	+381	-350	-8	+24
2tP	-157	-3170	-71	-3398
2cNP	113	-3455	-75	-3417
c/t difference	+270	-285	-4	-19
2cOP	-26	-3312	-66	-3404
c/c difference	-139	+143	+9	+13

Table 2 The results of Kitaura-Morokuma-Ziegler-Rauk energy decomposition analysis[12,13] in kJ mol^{-1} for the NBE complexes of $Pd^{II}(CN)(COOMe)(PPh_3)$ (steric energy is the sum of electrostatic and Pauli repulsion terms, orbital energy is the sum of kinetic, Coulomb, and exchange/correlation terms using BHandHLYP functional, bonding is the sum of steric, orbital, and solvation energies).

Complex	Complex formation				NBE dissociation			
	Steric	Orbital	Solv.	Bonding	Steric	Orbital	Solv.	Bonding
exo-**3tP-O**	-1418	-2288	-54	-3761	-361	483	-11	111
exo-**3tP-N**	-1463	-2229	-53	-3745	-245	357	-13	98
exo-**3cNP**	-44	-3332	-70	-3447	-102	185	-2	81
exo-**3cOP**	-193	-3172	-72	-3438	-232	380	-16	133
endo-**3tP-O**	-315	-3052	-63	-3430	-172	249	-12	64
endo-**3tP-N**	-312	-3058	-63	-3433	-187	268	-14	68
endo-**3cNP**	63	-3421	-68	-3426	-51	96	-4	41
endo-**3cOP**	-166	-3176	-69	-3412	-163	278	-16	99

The origin of exclusive *exo*-selectivity in the Pd-catalyzed cyanoesterification reaction of methyl cyanoformate is attributed from decisive energy gap between *exo*- and *endo*-coordination of norbornene to Pd^{II} 14-electron, coordinatively unsaturated complex.